






## Article

# Eco-Friendly Mechanochemical Preparation of Ag<sub>2</sub>O–MnO<sub>2</sub>/Graphene Oxide Nanocomposite: An Efficient and Reusable Catalyst for the Base-Free, Aerial Oxidation of Alcohols

Syed Farooq Adil <sup>1,\*</sup> , Mohamed E. Assal <sup>1</sup>, Mujeeb Khan <sup>1</sup> , Mohammed Rafi Shaik <sup>1</sup> , Mufsir Kuniyil <sup>1</sup> , Doumbia Sekou <sup>1</sup>, Ahmed Z. Dewidar <sup>2</sup>, Abdulrahman Al-Warthan <sup>1</sup> and Mohammed Rafiq H. Siddiqui <sup>1,\*</sup> 

<sup>1</sup> Chemistry Department, College of Science, King Saud University, P.O. 2455, Riyadh 11451, Saudi Arabia; masl@ksu.edu.sa (M.E.A.); kmujeeb@ksu.edu.sa (M.K.); mrshaik@ksu.edu.sa (M.R.S.); mkuniyil@ksu.edu.sa (M.K.); sdoumbia333@gmail.com (D.S.); awarthan@ksu.edu.sa (A.A.-W.)

<sup>2</sup> Agricultural Engineering Department, King Saud University, P.O. Box 2460, Riyadh 11451, Saudi Arabia; adewidar@ksu.edu.sa

\* Correspondence: sfadil@ksu.edu.sa (S.F.A.); rafiqs@ksu.edu.sa (M.R.H.S.)

Received: 5 February 2020; Accepted: 19 February 2020; Published: 1 March 2020



**Abstract:** Recently, the development of eco-friendly mechanochemical approaches for the preparation of novel catalysts with enhanced activity and selectivity has gained considerable attention. Herein, we developed a rapid and solvent-less mechanochemical method for the preparation of mixed metal oxide (Ag<sub>2</sub>O–MnO<sub>2</sub>) decorated graphene oxide (GRO)-based nanocomposites (Ag<sub>2</sub>O–MnO<sub>2</sub>/(X wt.%)GRO), as the Ag<sub>2</sub>O–MnO<sub>2</sub>/(X wt.%)GRO nanocomposite was fabricated by the physical grinding of freshly prepared GRO and pre-annealed (300 °C) mixed metal oxide nanoparticles (NPs) (Ag<sub>2</sub>O–MnO<sub>2</sub>) using an eco-friendly milling procedure. The as-prepared nanocatalysts were characterized by using various techniques. Furthermore, the nanocomposites were applied as a heterogeneous catalyst for the oxidation of alcohol by employing gaseous O<sub>2</sub> as an eco-friendly oxidant under base-free conditions. The mechanochemically obtained GRO-based composite exhibited noticeable enhancement in the surface area and catalytic performance compared to the pristine Ag<sub>2</sub>O–MnO<sub>2</sub>. The results revealed that (1%)Ag<sub>2</sub>O–MnO<sub>2</sub>/(5 wt.%)GRO catalyst exhibited higher specific performance (13.3 mmol·g<sup>−1</sup>·h<sup>−1</sup>) with a 100% conversion of benzyl alcohol (BnOH) and >99% selectivity towards benzaldehyde (BnH) within 30 min. The enhancement of the activity and selectivity of GRO-based nanocatalyst was attributed to the presence of various oxygen-containing functional groups, a large number of defects, and a high specific surface area of GRO. In addition, the as-prepared nanocatalyst also demonstrated excellent catalytic activity towards the conversion of a variety of other alcohols to respective carbonyls under optimal conditions. Besides, the catalyst ((1%)Ag<sub>2</sub>O–MnO<sub>2</sub>/(5 wt.%)GRO) could be efficiently recycled six times with no noticeable loss in its performance and selectivity.

**Keywords:** Ag<sub>2</sub>O nanoparticles; graphene oxide; nanocomposite; MnO<sub>2</sub>; oxidation; catalyst

## 1. Introduction

Catalytic oxidation of alcohol to their analogous carbonyls is one of the key organic reactions in both scientific and industrial applications, with universal production of 10,000 million tons/year of carbonyls in the 20th century [1]. Such as, aldehyde and ketone derivatives are extensively employed as precursors in insecticide, flame-retardant, cosmetic, confectionery, flavoring, pharmaceutical, and beverage industries [2]. Traditionally, the current oxidation process depends on the utilization of

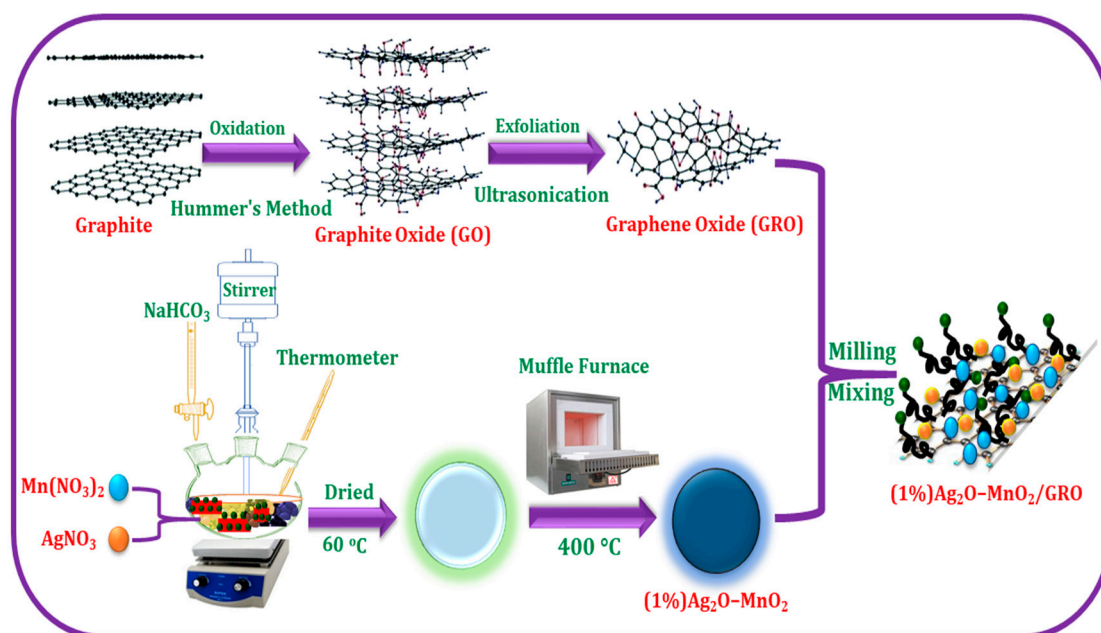
strong stoichiometric oxidizing agents, which are usually expensive and toxic (e.g., permanganate, hypochlorite, or dichromate, etc.) [3]. Moreover, the strong nature of these conventional oxidizing agents leads to an over-oxidation of alcohols to  $\text{CO}_2$  or carboxylic acids, thus decreasing the selectivity towards aldehydes [4]. Alternatively, due to the growing environmental concerns, the applications of eco-friendly oxidants, such as molecular  $\text{O}_2$  and aqueous  $\text{H}_2\text{O}_2$ , have been preferred, which only produces water as the by-product [5].

Moreover, graphene-based materials have also attracted increasing attention in the field of catalysis due to their extraordinary optical, electronic, and catalytic properties [6]. The unique 2D structure of graphene allows introducing a variety of functionalities on its surface through covalent and non-covalent interactions [7]. This property can be successfully exploited for the development of graphene-based sustainable catalysts [8]. In this regard, the precursors of graphene, i.e., graphene oxide (GRO)-based materials, have generated significant excitement in the field of catalysis due to their remarkable physicochemical and surface properties [9]. Particularly, the presence of a variety of oxygenated groups, a large number of defects, and a unique 2D structure have rendered graphene oxide as perfect material in catalysis [10]. In addition, the negatively charged surface of GRO can be easily exploited for the dispersion of other catalytically active materials, including metal and metal oxide nanoparticles (NPs), on its surface to enhance their resulting properties [11,12]. Several metal and/or metal oxide NPs like Pd [13], Ag [14],  $\text{Co}_3\text{O}_4$  [15],  $\text{ZrO}_2$  [16], and  $\text{Fe}_2\text{O}_3$  [17] have incorporated on GRO nanolayers and achieved superior performance and selectivity. Recently, GRO-based metal nanocomposites have been explored and exhibited considerable potential in the oxidation of various organic moieties, including alcohols [18], cyclohexane [19], amines [20], benzene [21], aryl benzene [22], and alkenes [23]. It has been found that the GRO in these nanocomposites has a positive impact in enhancing the catalytic efficiency and selectivity.

The methods for the binding of nanomaterials on the surface of GRO are broadly classified in two different categories, i.e., post immobilization (ex-situ hybridization) and in situ binding (in-situ crystallization). In the post immobilization method, separately prepared dispersions of graphene or graphene oxide and pre-synthesized NPs are mixed to obtain nanocomposite, whereas in-situ binding is performed by the simultaneous reduction of graphene oxide and metal precursors [24]. So far, several methods have been reported for the synthesis of graphene-based nanocomposites, including chemical, electrochemical, microwave-based synthesis, etc. Among these methods, the chemical method is widely used for the large-scale synthesis of graphene-based nanocomposites. However, this method typically involves hazardous chemicals and functionalization ligands, which often have adverse effects on the environment. This gave the impetus to researchers to find alternative eco-friendly methods for the synthesis of graphene-based nanocomposites [25]. Recently, environmentally friendly mechanochemical preparation methods have emerged as a suitable alternative to the commonly applied chemical approaches for the preparation of nanomaterials with outstanding properties for advanced applications. Nowadays, these methods are also gaining significant popularity for the preparation of graphene-based nanocomposites [26]. For instance, in a recent study, Zhao et al. demonstrated the preparation of  $\text{FeO}(\text{OH})$ -nanoflake/graphene and nano- $\text{Fe}_3\text{O}_4$ /graphene composites using a simple and low-cost solid-state mechanochemical process [27].

Herein, we reported the eco-friendly fabrication of  $\text{Ag}_2\text{O-MnO}_2/\text{GRO}$  nanocomposites by the solid-state mixing of separately prepared GRO and  $\text{Ag}_2\text{O-MnO}_2$  NPs using a mechanochemical ball milling method. The as-obtained catalysts were fully characterized using X-ray powder diffraction (XRD), High-resolution transmission electron microscopy (HR-TEM), Scanning electron microscope (SEM), Energy-dispersive X-ray spectroscopy (EDX), Brunauer–Emmett–Teller (BET), Thermal gravimetric analysis (TGA), Fourier-transform infrared spectroscopy (FTIR), and Raman spectroscopy. Subsequently, to study the catalytic effect of GRO, the as-prepared catalysts were tested towards the aerial oxidation of a variety of alcohols, as displayed in Scheme 1. To the best of our knowledge, this was the first study of utilizing  $\text{Ag}_2\text{O-MnO}_2/\text{GRO}$  composite as a catalyst for the oxidation of alcohols, highlighting the catalytic efficiency of GRO. The catalytic activity

of  $\text{Ag}_2\text{O-MnO}_2/\text{GRO}$  nanocomposite was also compared with the highly reduced graphene oxide (HRG)-based catalyst that was prepared by the same protocol reported earlier, i.e.,  $\text{Ag}_2\text{O-MnO}_2/\text{HRG}$  nanocomposite, and the conclusions were drawn [28].



**Scheme 1.** Fabrication of  $(1\%)\text{Ag}_2\text{O-MnO}_2/\text{GRO}$  nanocomposite. GRO: graphene oxide.

## 2. Results and Discussion

### 2.1. Characterizations

XRD analysis is an imperative technique to study the crystallinity of the synthesized samples. Figure 1 illustrates XRD patterns of the pure graphite, GRO,  $(1\%)\text{Ag}_2\text{O-MnO}_2$  (without GRO), and  $(1\%)\text{Ag}_2\text{O-MnO}_2/(5 \text{ wt.}\%)\text{GRO}$  nanocomposite. Pure graphite exhibited an intensive diffraction peak at  $2\theta = 26.5^\circ$  (cf. Figure 1, green line), which corresponded to the (0 0 2) lattice plane with an interlayer spacing of approximately  $3.4 \text{ \AA}$  [29]. The appearance of a diffraction peak at  $2\theta = 11.6^\circ$  (cf. Figure 1, cyan line) corresponded to the (002) lattice plane of GRO, and the disappearance of characteristic graphite peak at  $2\theta = 26.5^\circ$  confirmed the complete oxidation of graphite to GRO [30]. After the oxidation, the interlayer distance of graphite was increased to  $6.4 \text{ \AA}$  due to the existence of oxygenated groups on the surface and edges of each nanosheet [31]. The XRD spectrum of  $(1\%)\text{Ag}_2\text{O-MnO}_2$  (without GRO, Figure 1 orange line) contained characteristic diffraction peaks of pyrolusite  $\text{MnO}_2$ , which were in complete agreement with the published data of JCPDS file no. 24-0735 [32]. On the other hand, the  $(1\%)\text{Ag}_2\text{O-MnO}_2/(5 \text{ wt.}\%)\text{GRO}$  nanocomposite possessed all the diffraction peaks corresponding to the  $(1\%)\text{Ag}_2\text{O-MnO}_2$ , and, in addition, it also contained the characteristic (002) peak of GRO at  $11.6^\circ$  (cf. Figure 1, blue line), confirming the formation of nanocomposite.

The thermal stability of  $(1\%)\text{Ag}_2\text{O-MnO}_2/(5 \text{ wt.}\%)\text{GRO}$  nanocomposite had been compared with the thermal properties of the precursors, like pure graphite, GRO, and  $(1\%)\text{Ag}_2\text{O-MnO}_2$  utilizing TGA, as shown in Figure 2. The samples were heated between RT and  $800^\circ\text{C}$  with  $10^\circ\text{C}/\text{minute}$  heating rate in  $\text{N}_2$  atmosphere. The TGA graph of graphite exhibited only  $\sim 1\%$  of weight loss [33]. On the contrary, the thermal degradation behavior of GRO was significantly lower compared to the graphite due to the existence of oxygen functionalities on the surface of GRO. GRO exhibited three steps of degradation. The first weight loss began at nearly  $100^\circ\text{C}$ , which was ascribed to the evaporation of physisorbed  $\text{H}_2\text{O}$ . The second thermal degradation occurred in the temperature range of  $200\text{--}370^\circ\text{C}$  with a noticed weight loss of  $43.5\%$  due to the pyrolysis of labile oxygen-containing functionalities,

such as CO, CO<sub>2</sub>, etc. The third degradation stage occurred in the range of 350–800 °C, with 11% weight loss attributed to the combustion of the residual carbonaceous skeleton of the graphene layer [34]. This data was in complete agreement with previously reported studies [31,35]. In comparison, the (1%)Ag<sub>2</sub>O–MnO<sub>2</sub>/(5 wt.%)GRO composite exhibited a much enhanced thermal stability, which lost only ~18% of its overall weight at 800 °C (cf. Figure 2, purple line), probably owing to the pyrolysis of GRO when exposed to an elevated temperatures [36]. This indicated the high stability of the (1%)Ag<sub>2</sub>O–MnO<sub>2</sub>/(5 wt.%)GRO composite when compared to pristine GRO and (1%)Ag<sub>2</sub>O–MnO<sub>2</sub> NPs; however, it was slightly less stable than pure graphite.

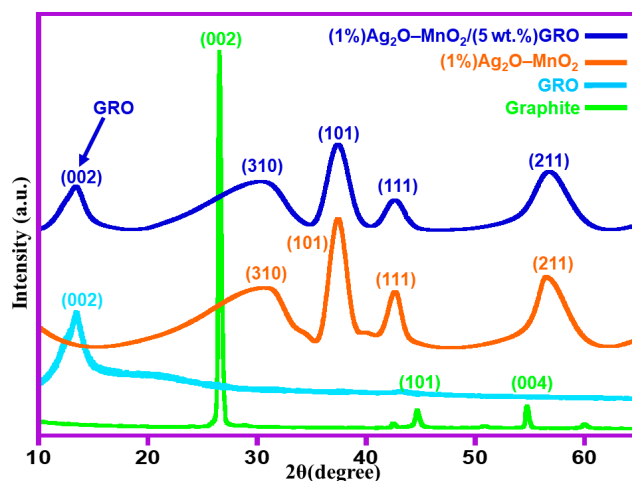


**Figure 1.** XRD analysis of the graphite, GRO, (1%)Ag<sub>2</sub>O–MnO<sub>2</sub>, and (1%)Ag<sub>2</sub>O–MnO<sub>2</sub>/(5 wt.%)GRO. GRO: graphene oxide.

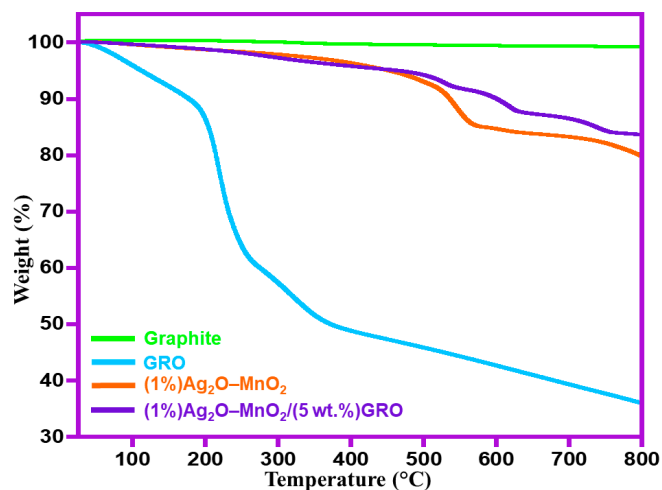


**Figure 2.** TGA graphs of the graphite, GRO, (1%)Ag<sub>2</sub>O–MnO<sub>2</sub>, and (1%)Ag<sub>2</sub>O–MnO<sub>2</sub>/(5 wt.%)GRO.

Raman analyses were also performed for the samples, including GRO, (1%)Ag<sub>2</sub>O–MnO<sub>2</sub>, and (1%)Ag<sub>2</sub>O–MnO<sub>2</sub>/(5 wt.%)GRO, as displayed in Figure 3. The Raman spectra of the (1%)Ag<sub>2</sub>O–MnO<sub>2</sub> and (1%)Ag<sub>2</sub>O–MnO<sub>2</sub>/(5 wt.%)GRO nanocomposite exhibited a characteristic peak centered at 642 cm<sup>−1</sup>. The presence of this peak could be attributed to the symmetric lattice vibration of Mn–O, which pointed towards the existence of manganese dioxide in both (1%)Ag<sub>2</sub>O–MnO<sub>2</sub> and (1%)Ag<sub>2</sub>O–MnO<sub>2</sub>/(5 wt.%)GRO nanocomposite [37]. Additionally, the Raman spectra of the composite also possessed two different characteristic peaks of GRO at 1594 cm<sup>−1</sup> and 1340 cm<sup>−1</sup>, which were assigned to D- and G-band of GRO, respectively [38]. On the other hand, the pristine GRO possessed G- and the D-bands at 1604 cm<sup>−1</sup> and 1345 cm<sup>−1</sup>, respectively [39]. Notably, when compared to the pristine GRO, the G-band in nanocomposite was

shifted  $\sim 10\text{ cm}^{-1}$  from  $1604\text{ cm}^{-1}$  to  $1594\text{ cm}^{-1}$ , while a small shift was detected in the D-band from  $1345\text{ cm}^{-1}$  to  $1340\text{ cm}^{-1}$ . These small shifts could be attributed to the interaction between  $\text{MnO}_2$  and GRO [40].

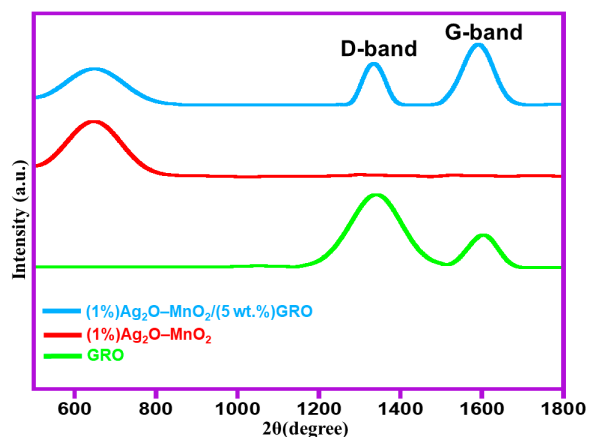


**Figure 3.** Raman spectra of GRO, (1%) $\text{Ag}_2\text{O-MnO}_2$ , and (1%) $\text{Ag}_2\text{O-MnO}_2/(5\text{ wt.}\%)\text{GRO}$ .

The morphology and particle size of GRO, (1%) $\text{Ag}_2\text{O-MnO}_2$ , and (1%) $\text{Ag}_2\text{O-MnO}_2/(5\text{ wt.}\%)\text{GRO}$  nanocomposite were analyzed by HR-TEM. Figure 4a demonstrates highly exfoliated GRO nanolayers, which had a transparent thin flake morphology. HR-TEM images of the synthesized (1%) $\text{Ag}_2\text{O-MnO}_2/(5\text{ wt.}\%)\text{GRO}$  nanocomposite distinctly disclosed that the size of the  $\text{Ag}_2\text{O}$  nanoparticles in the catalyst with  $0.83 \pm 0.12\text{ nm}$  as average size with spherical shape was well dispersed on the crumpled GRO nanolayers, as demonstrated in Figure 4c,d. Notably, the HR-TEM micrograph of the (1%) $\text{Ag}_2\text{O-MnO}_2$  without GRO showed the average diameter of  $\text{Ag}_2\text{O}$  NPs in the range of  $2.09 \pm 0.35\text{ nm}$ , which was larger than the  $\text{Ag}_2\text{O}$  NPs present in the composite, as displayed in Figure 4b [6]. Presumably, the mechanochemical forces applied during the ball milling process facilitated the formation of the smaller size of NPs in the composite. The presence of smaller size of NPs in the composite, as confirmed by the HR-TEM analysis, was also reflected by the enhanced surface area and catalytic activity of sample when compared to the (1%) $\text{Ag}_2\text{O-MnO}_2$ .

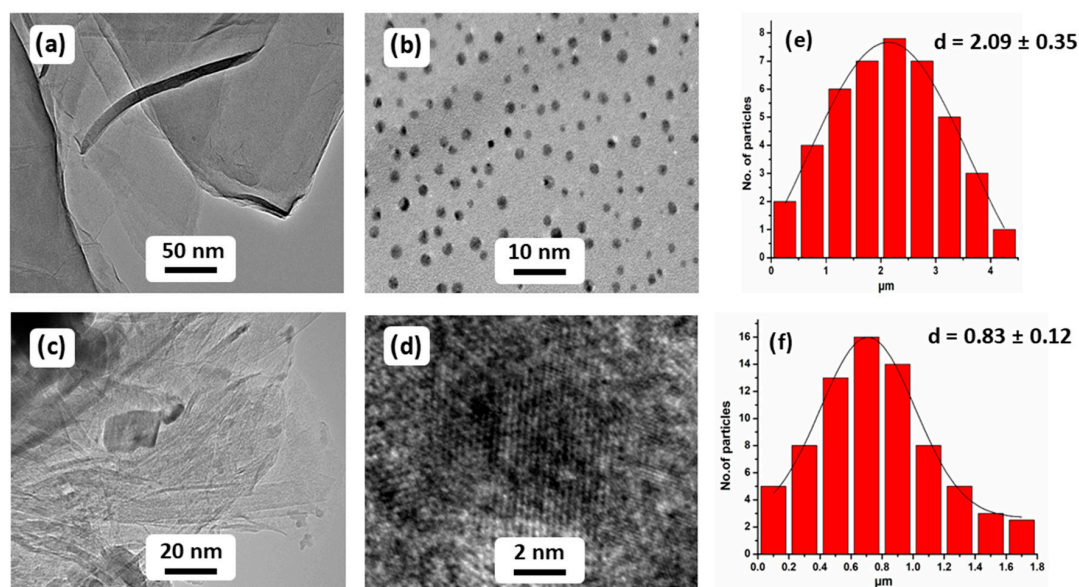


**Figure 4.** HR-TEM images of (a) GRO, (b) (1%) $\text{Ag}_2\text{O-MnO}_2$  catalyst (without GRO), (c,d) (1%) $\text{Ag}_2\text{O-MnO}_2/(5\text{ wt.}\%)\text{GRO}$  nanocomposite, (e,f) particle size distribution of (1%) $\text{Ag}_2\text{O-MnO}_2$  and (1%) $\text{Ag}_2\text{O-MnO}_2/(5\text{ wt.}\%)\text{GRO}$  nanocomposite, correspondingly.



The morphology of the as-prepared (1%)Ag<sub>2</sub>O–MnO<sub>2</sub> and (1%)Ag<sub>2</sub>O–MnO<sub>2</sub>/(5 wt.%)GRO nanocomposite was also examined by SEM, as displayed in Figure 5. The SEM micrographs of the catalyst without GRO, i.e., (1%)Ag<sub>2</sub>O–MnO<sub>2</sub>, showed well-defined cuboidal shaped particles with micro size. Whereas, the nanocomposite displayed much smaller cuboidal shaped microparticles due to ball mill process. The nanoparticles after ball milling caused a smaller but wide size distribution. This led to an increase in the total surface area of the catalyst. In addition, the elemental results of the obtained (1%)Ag<sub>2</sub>O–MnO<sub>2</sub>/(5 wt.%)GRO by means of EDX are also illustrated in Figure 6. The figure clearly showed the presence of Ag, Mn, O, and C in the sample.

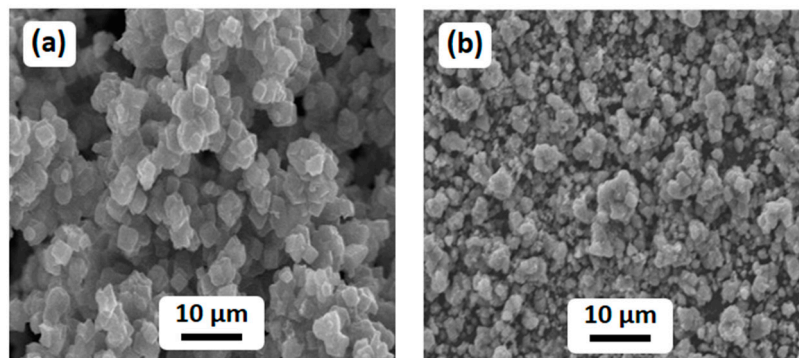


Figure 5. SEM analysis of (a) (1%)Ag<sub>2</sub>O–MnO<sub>2</sub> and (b) (1%)Ag<sub>2</sub>O–MnO<sub>2</sub>/(5 wt.%)GRO nanocomposite.

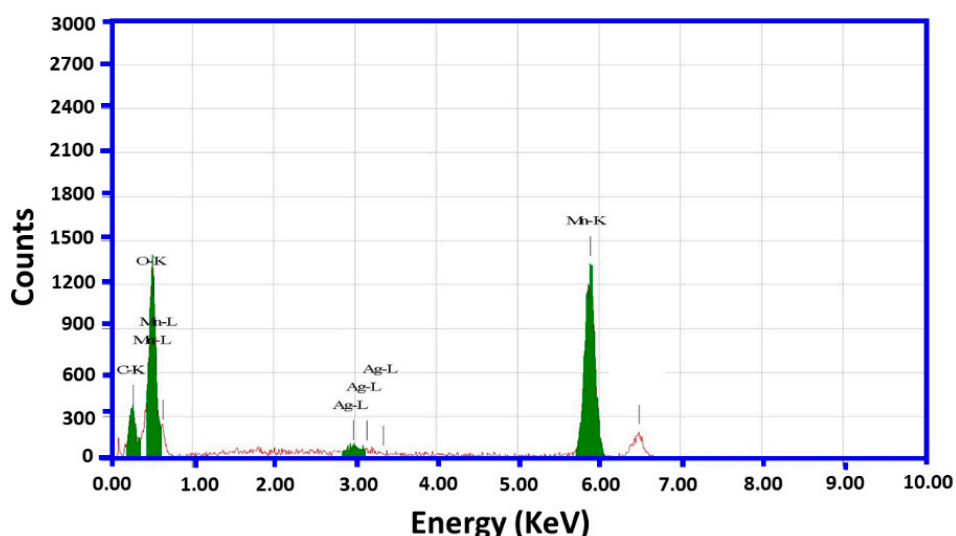


Figure 6. EDX spectrum of the (1%)Ag<sub>2</sub>O–MnO<sub>2</sub>/(5 wt.%)GRO nanocomposite.

Furthermore, the BET analysis revealed the surface area of the samples; the surface area of (1%)Ag<sub>2</sub>O–MnO<sub>2</sub> (without GRO) was approximately 84 m<sup>2</sup>.g<sup>−1</sup>, as demonstrated in Table 1. Whereas, the nanocomposite after doping with GRO demonstrated an enhanced surface area of 158 m<sup>2</sup>.g<sup>−1</sup>. These results were in good agreement with the results of SEM and TEM analyses, which revealed the presence of small-sized nanoparticles in the composite. Hence, it was assumed that the preparation of (1%)Ag<sub>2</sub>O–MnO<sub>2</sub>/(5 wt.%)GRO by the induction of GRO through an eco-friendly mechanochemical process leads to the formation of a stable and efficient nanocatalyst.

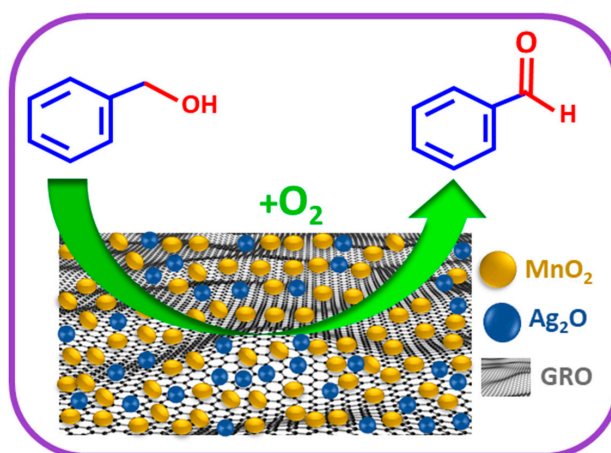
**Table 1.** Catalytic oxidation of BnOH, catalyzed by different catalysts.

Entry	Catalyst	Surface Area (m <sup>2</sup> .g <sup>-1</sup> )	Conv. (%)	Sp. Performance (mmol.g <sup>-1</sup> .h <sup>-1</sup> )	Sel. (%)
1	GRO	85.4	3.2	0.43	<99
2	HRG	78.2	3.0	0.39	<99
3	MnO <sub>2</sub>	39.3	40.7	5.4	<99
4	(1%)Ag <sub>2</sub> O–MnO <sub>2</sub>	84.3	65.0	8.6	<99
5	(1%)Ag <sub>2</sub> O–MnO <sub>2</sub> /(5 wt.%)HRG	149.1	94.1	12.5	<99
6	(1%)Ag <sub>2</sub> O–MnO <sub>2</sub> /(5 wt.%)GRO	158.7	100.0	13.3	<99

**Conditions:** 300 mg catalyst, 15 mL toluene, 20 mL.min<sup>-1</sup> O<sub>2</sub> rate, 2 mmol BnOH, 100 °C, 30 min. HRG: highly reduced graphene oxide.

## 2.2. Catalytic Assessment

To assess the catalytic efficacy of the as-prepared nanocomposites, oxidation of benzyl alcohol (BnOH) utilizing molecular O<sub>2</sub> as an eco-friendly oxidizing agent was employed as a model substrate, as demonstrated in Scheme 2. Various catalysts were fabricated by changing the weight percentage of GRO in the nanocomposite. In addition, the influence of catalyst weight, reaction temperature, and time on the performance of the prepared catalysts was thoroughly examined to determine the optimum conditions, as demonstrated in Figures 7–10 and Tables 1 and 2.



**Scheme 2.** Schematic representation of benzyl alcohol (BnOH) oxygenation, employing O<sub>2</sub> over the prepared nanocomposite.

### 2.2.1. Influence of wt% GRO

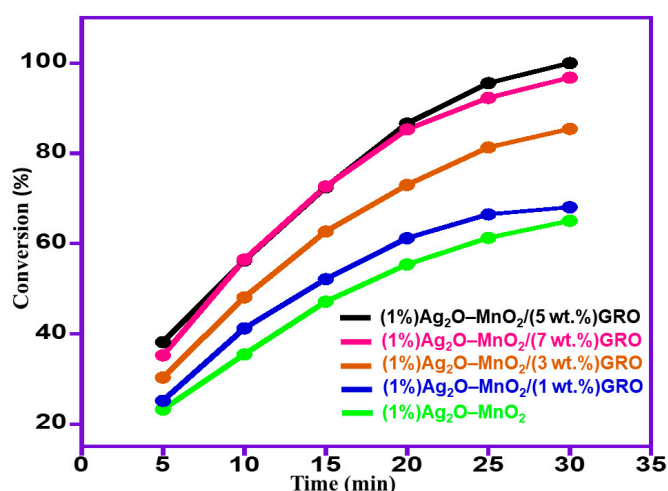
The efficacy of the catalytic performance could be enhanced using graphene or its derivatives as supporting material and an efficient promoter [41,42]. Previously, we showed that the silver oxide nanoparticles were an efficacious promoter to the manganese dioxide, and the (1%)Ag<sub>2</sub>O–MnO<sub>2</sub> catalyst annealed at 400 °C, exhibiting the superior activity for aerial oxidation of alcohols employing gaseous O<sub>2</sub> as a clean oxidizing agent [32]. Therefore, herein, the (1%)Ag<sub>2</sub>O–MnO<sub>2</sub> catalyst was selected with a target to compare the support effects. However, in order to enhance the catalytic efficiency, the initial studies were done to know the convenient weight percentage of GRO (wt.%) in the synthesized nanocomposite.

First of all, we tested the performance of pure GRO (300 g) for the aerial oxidation of BnOH with O<sub>2</sub> as an environmentally-friendly oxidant. It was found that the GRO was not active for the BnOH oxidation. However, when the various weight percentages of GRO were introduced to the prepared nanocomposite, i.e., (1%)Ag<sub>2</sub>O–MnO<sub>2</sub>/(X wt.%)GRO (X = 1–7), it was found to have a strong impact on the catalytic efficacy. The obtained results from the catalytic tests are summed up in Table 2 and plotted in Figure 7.

**Table 2.** Oxidation of BnOH using several wt.% of GRO.

Entry	Catalyst	Conv. (%)	Sp. Performance (mmol.g <sup>-1</sup> .h <sup>-1</sup> )	Sel. (%)
1	GRO	3.2	0.43	<99
2	(1%)Ag <sub>2</sub> O–MnO <sub>2</sub>	65.0	8.6	<99
3	(1%)Ag <sub>2</sub> O–MnO <sub>2</sub> /(1 wt.%)GRO	68.1	9.1	<99
4	(1%)Ag <sub>2</sub> O–MnO <sub>2</sub> /(3 wt.%)GRO	85.4	11.3	<99
5	(1%)Ag <sub>2</sub> O–MnO <sub>2</sub> /(5 wt.%)GRO	100.0	13.3	<99
6	(1%)Ag <sub>2</sub> O–MnO <sub>2</sub> /(7 wt.%)GRO	96.8	12.9	<99

**Conditions:** 300 mg catalyst, 20 mL.min<sup>-1</sup> O<sub>2</sub> rate, 15 mL toluene, 2 mmol BnOH, 100 °C, 30 min. BnOH: benzyl alcohol; GRO: graphene oxide.

**Figure 7.** Graphical representation of BnOH oxidation, using catalysts with various percentages of GRO.

As seen in Table 2 and Figure 7, the catalyst without GRO ((1%)Ag<sub>2</sub>O–MnO<sub>2</sub>) afforded a 65% BnOH conversion within only 30 min. However, after doping of the prepared catalyst with 1 and 3 wt.% of GRO, i.e., (1%)Ag<sub>2</sub>O–MnO<sub>2</sub>/(1 wt.%)GRO and (1%)Ag<sub>2</sub>O–MnO<sub>2</sub>/(3 wt.%)GRO, the nanocomposites yielded BnOH conversion of 68.1% and 85.4%, respectively, under the identical circumstances. By further increasing the wt.% of GRO in the nanocomposite, i.e., (1%)Ag<sub>2</sub>O–MnO<sub>2</sub>/(5 wt.%)GRO, the catalytic efficiency remarkably increased and gave a 100% conversion after 30 min in addition to 13.3 mmol.g<sup>-1</sup>.h<sup>-1</sup> specific performance. Further increase in the weight percentage of GRO led to a slight decline in the effectiveness of the nanocomposite, presumably ascribed to the blocking effect of GRO that could cover the active sites of the catalyst, owing to the high wt.% of GRO. Meanwhile, the benzaldehyde (BnH) selectivity still remained motionless during all oxidation processes (<99%). Accordingly, it was deduced that the GRO had a crucial influence in promoting the performance of the current catalytic strategy for this transformation.

## 2.2.2. Role of Various Graphene Supports

Based on our former reported publications, we also compared the efficiency of Ag<sub>2</sub>O NPs/MnO<sub>2</sub> immobilized on various graphene supports, such as GRO, and highly reduced graphene oxide (HRG) for the oxidation of BnOH to understand the role of graphene. The obtained data are compiled in Table 1 and depicted in Figure 8. As displayed in Table 1, the MnO<sub>2</sub> without Ag<sub>2</sub>O NPs yielded a 40.7% BnOH conversion after 30 min, while after doping it with 1 wt.% of Ag<sub>2</sub>O NPs in MnO<sub>2</sub>, i.e., (1%)Ag<sub>2</sub>O–MnO<sub>2</sub>, the performance significantly improved and gave 65% conversion of BnOH under the same circumstances. This was further raised to 100% conversion when 5 wt.% of GRO was utilized, i.e., (1%)Ag<sub>2</sub>O–MnO<sub>2</sub>/(5 wt.%)GRO nanocomposite. This catalyst showed remarkably higher catalytic activity, giving a full BnOH conversion within only 30 min.



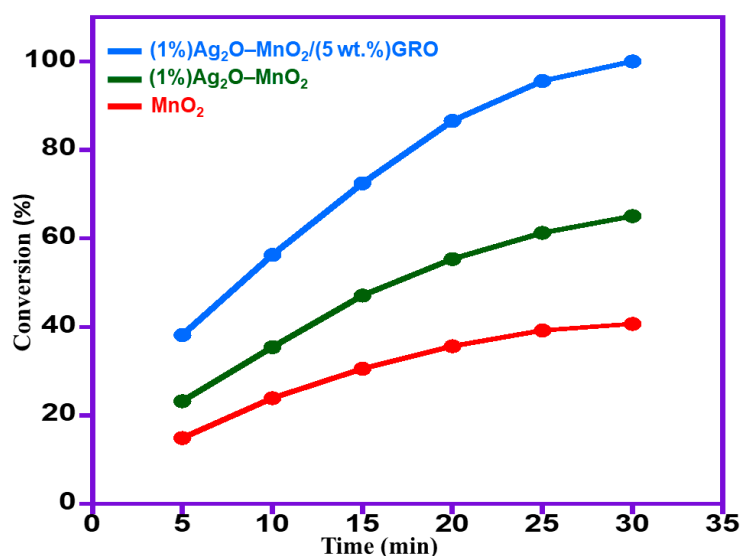


Figure 8. Impact of time on catalytic performances of fabricated catalysts.

It is interesting to note that the catalytic activity of HRG-based catalyst protocol, i.e., (1%)Ag<sub>2</sub>O-MnO<sub>2</sub>/(5 wt.%)HRG nanocomposite, reported earlier was compared with the catalytic efficacy of the (1%)Ag<sub>2</sub>O-MnO<sub>2</sub>/(5 wt.%)GRO nanocomposite [28]. It was found that the (1%)Ag<sub>2</sub>O-MnO<sub>2</sub>/(5 wt.%)HRG showed lower catalytic efficiency, which afforded a 94.1% conversion of BnOH alongside 12.5 mmol·g<sup>-1</sup>·h<sup>-1</sup> specific performance within 30 min at 100 °C, while (1%)Ag<sub>2</sub>O-MnO<sub>2</sub>/(5 wt.%)GRO gave 100% conversion with 13.3 mmol·g<sup>-1</sup>·h<sup>-1</sup> specific performance under similar circumstances. The higher activity of the catalyst could be attributed to the addition of GRO, which might provide additional defects/nucleation sites (which possesses abundant oxygen-carrying groups on the surface of GRO) to the catalytic nanocomposite along with the already existing active sites of Ag<sub>2</sub>O NPs-MnO<sub>2</sub>. Nevertheless, with respect to HRG, the nucleation sites were less in number that resulted in more aggregated growth of an active catalyst. In addition, the specific surface area of GRO-based nanocomposite was higher than that of HRG nanocomposite. Therefore, it could be stated that utilizing GRO for synthesizing the metallic oxide catalysts could be useful for the homogeneous growth of catalyst on the surface.

### 2.2.3. Impact of Temperature

In general, the temperature played an important role in the catalytic system and had an obvious impact on the catalytic efficacy of the catalyst. Therefore, a series of reactions were carried out at different temperatures, viz. RT, 40, 60, 80, and 100 °C, catalyzed by MnO<sub>2</sub>, (1%)Ag<sub>2</sub>O-MnO<sub>2</sub>, and (1%)Ag<sub>2</sub>O-MnO<sub>2</sub>/(5 wt.%)GRO by maintaining other factors constant. The data presented in Figure 9 showed that the temperature had a positive effect on the effectiveness of all catalysts employed in the present study. While the selectivities to BnH were achieved <99% for all catalysts.

Figure 9 shows that the optimum catalyst showed the highest activity in the (1%)Ag<sub>2</sub>O-MnO<sub>2</sub>/(5 wt.%)GRO catalyst. At RT, a lower alcohol conversion of 38.2% was obtained. Unsurprisingly, the elevated reaction temperatures assisted in the higher catalytic efficiency of the catalyst. At 100 °C, a 100% transformation of alcohol was achieved under the same catalytic circumstances. Consequently, 100 °C could be considered as the optimum reaction temperature for a higher conversion rate. Hence, it was selected for further studies.

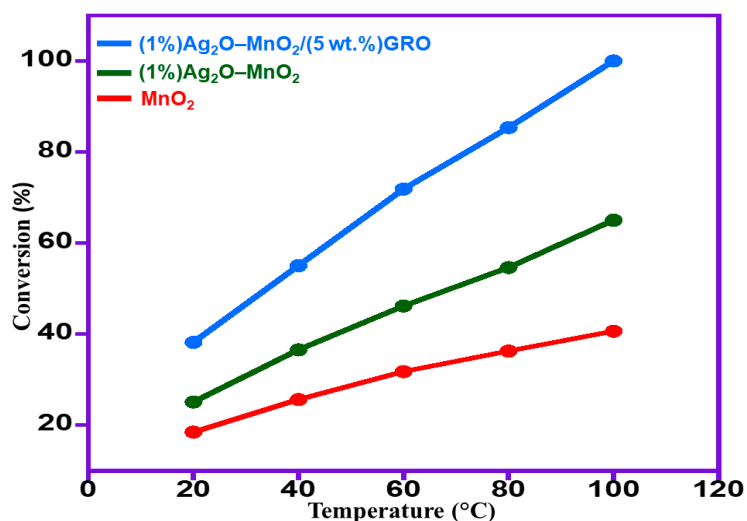


Figure 9. Impact of temperature on the benzyl alcohol (BnOH) conversion using various catalysts.

#### 2.2.4. Impact of Catalyst Dosage

To evaluate the influence of varying amount of catalysts (MnO<sub>2</sub>, (1%)Ag<sub>2</sub>O-MnO<sub>2</sub>, and (1%)Ag<sub>2</sub>O-MnO<sub>2</sub>/(5 wt.%)GRO), six different quantities (50, 100, 150, 200, 250, and 300 mg) were taken with keeping all other factors constant, and the attained catalytic data were plotted, as shown in Figure 10. It clearly shows that BnOH conversion increased linearly as the catalyst doses raised from 50 mg to 300 mg. However, the selectivity to aldehyde was almost motionless throughout the oxidation processes (<99%). Among all catalysts employed in this study, the (1%)Ag<sub>2</sub>O-MnO<sub>2</sub>/(5 wt.%)GRO catalyst showed superior activity towards BnOH oxidation; when the catalyst amount raised from 50 mg to 300 mg, the conversion of BnOH markedly increased from 29.9% to 100% after 30 min. The current study demonstrated that only 300 mg of the catalyst was needed for accomplishing the complete conversion of BnOH after a short period.

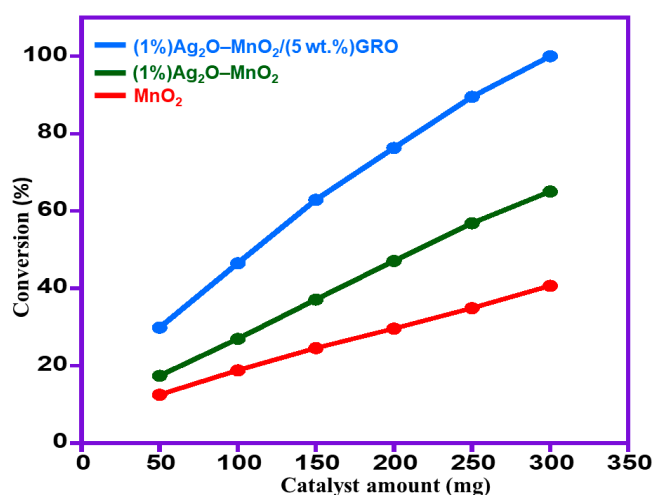


Figure 10. Impact of catalyst quantity on the oxidation of BnOH using various catalysts.

Under the optimum conditions, a blank test (without reactant, i.e., BnOH) was performed using (1%)Ag<sub>2</sub>O-MnO<sub>2</sub>/(5 wt.%)GRO catalyst in the presence of the solvent, i.e., toluene, to assure that there was no function of solvent in BnOH oxidation. However, no oxidative product (BnH) was detected, implying that the BnH was only produced from the catalytic oxidation of BnOH and not from toluene oxidation. Additionally, a blank test (no catalyst) was also carried out at the optimized circumstances to ascertain that the produced BnH was being obtained, owing to the catalytic efficacy of

the fabricated catalyst. No BnH was noticed, proving that the synthesized catalyst was indispensable for this transformation. Furthermore, to illustrate the importance of the oxidizing agent ( $O_2$ ), the experiment was performed over (1%) $Ag_2O$ - $MnO_2$ /(5 wt.%)GRO catalyst using air without bubbling  $O_2$ . At the optimum circumstances, the obtained data displayed that only 31.8% conversion of BnOH was detected, which was much lesser than that of 100% convertibility achieved when the process was conducted using gaseous  $O_2$ .

### 2.3. Reusability Tests

Recyclability and stability of the catalyst is a significant aspect in the enhancement of heterogeneous catalysis systems for industrial applications. The reusability of the (1%) $Ag_2O$ - $MnO_2$ /(5 wt.%)GRO nanocomposite was investigated for the catalytic oxidation of BnOH at the optimal circumstances. The catalytic activities of the (1%) $Ag_2O$ - $MnO_2$ /(5 wt.%)GRO catalyst at different cycles for BnOH oxidation are illustrated in Figure 11. The reusability data disclosed that we were able to reuse the fabricated catalyst for six runs with no manifest loss in its performance after every cycle. The BnOH conversion decreased slightly from 100% to 90.46% after six recycling experiments, presumably ascribed to the mass loss through the retrieving step [43]. It was interesting to note that BnH selectivity stayed motionless (<99%) through all recycling reactions. The attained data displayed that our catalyst was resistant to deactivation in aerial oxidation of BnOH.

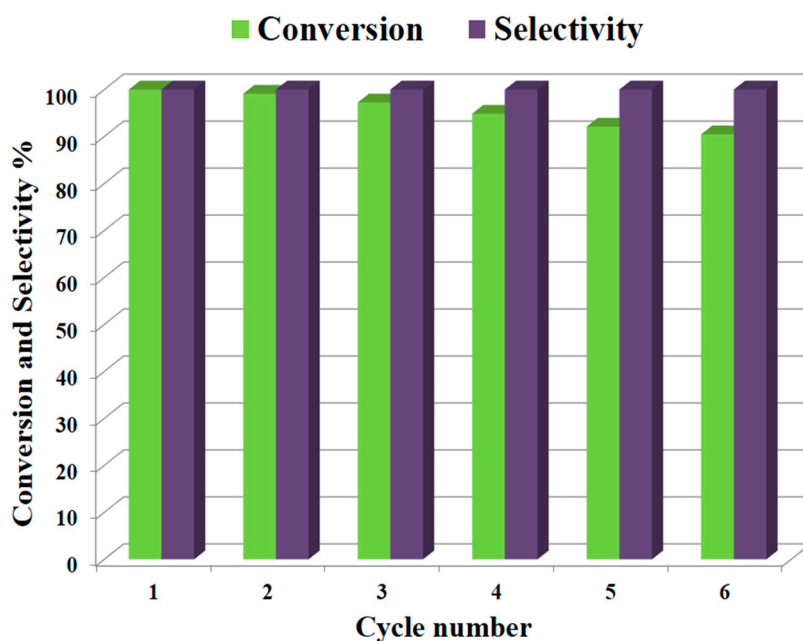


**Figure 11.** Reusability of (1%) $Ag_2O$ - $MnO_2$ /(5 wt.%)GRO catalyst for BnOH oxidation, **Conditions:** 300 g catalyst, 20 mL.min<sup>-1</sup>  $O_2$  rate, 15 mL toluene, 2 mmol BnOH, 100 °C, 30 min.

Moreover, to further elucidate the superior efficacy of the (1%) $Ag_2O$ - $MnO_2$ /(5 wt.%)GRO catalyst, this catalyst was compared with formerly recorded graphene containing catalysts, as displayed in Table 3. By comparing our catalyst with the other catalysts compiled in Table 3, (1%) $Ag_2O$ - $MnO_2$ /(5 wt.%)GRO catalyst, in this study, exhibited higher conversion and specific performance within shorter reaction time. Therefore, it could be said that our catalyst was the most efficient catalyst for BnOH oxidation with regard to higher conversion, selectivity, and specific performance, as well as lower reaction time. The (1%) $Ag_2O$ - $MnO_2$ /(5 wt.%)GRO nanocomposite afforded 100% BnOH conversion and <99% selectivity for BnH within 30 min alongside outstanding specific performance (13.3 mmol.g<sup>-1</sup>.h<sup>-1</sup>). For instance, Rana et al., [44] fabricated Cu supported amine-functionalized graphene oxide (Cu@AGO) and employed it for the catalytic oxidation of BnOH. The Cu@AGO catalyst gave 92% conversion and BnH selectivity (99%) with the specific performance of 2 mmol.g<sup>-1</sup>.h<sup>-1</sup> within 3 h. Feng et al., [45]

reported the employ of CuNPs@rGO composite as an effective catalyst for the BnOH oxidation, but it needed a relatively long reaction time (16 h) to give <99% conversion and 98.6% selectivity towards BnH alongside the lower specific performance of 8 mmol·g<sup>-1</sup>·h<sup>-1</sup>.

**Table 3.** Comparison of various graphene catalysts for selective oxidation of BnOH.

Catalyst	Conv. (%)	Sel. (%)	t.	T. (°C)	Sp. Performance (mmol·g <sup>-1</sup> ·h <sup>-1</sup> )	Ref.
Ag <sub>2</sub> O–MnO <sub>2</sub> /(5 wt.%)GRO	100	<99	30 min	100	13.3	This work
Ag <sub>2</sub> O–MnO <sub>2</sub> /(5 wt.%)HRG	94.1	<99	30 min	100	12.5	[28]
Cu@AGO	92	99	3 h	70	2.1	[44]
CuNPs@rGO	<99	98.6	16 h	80	8.3	[45]
Ru(CO)/NrGO	46	<99	24 h	90	6.4	[46]
AgNPs/GRO	33	55	24 h	80	2.8	[47]
AgNPs/rGO	12	8	24 h	80	1.0	[47]
Im-PW/GRO	90.8	99.2	7 h	90	8.6	[48]
Au/RGO	65	93	8 h	100	5.4	[43]
Pd NPs/GRO	36	34.1	6 h	110	1.0	[42]
1%RGO–MnCoO	78	100	2 h	140	12.6	[49]
GRO–N–PW	76	99	6 h	100	10.6	[50]
MnO <sub>2</sub> /GRO	97	100	3 h	110	1.6	[41]
Pd(II)-AAPTMS@GRO	96	99	3 h	60	2.1	[51]

#### 2.4. General Applicability

Moreover, Ag<sub>2</sub>O–MnO<sub>2</sub>/(5 wt.%)GRO was found to be an efficient and selective for the aerial oxidation of various kinds of alcohols, an indication of its considerable versatility. According to Table S1, all primary benzylic alcohols were easily oxidized to their respective aldehyde derivatives with 100% conversions within relatively short periods (Table S1, entries 1–20). Besides, perfect selectivities (<99%) toward respective aldehydes were accomplished for all alcohols used in this study without further oxidation to carboxylic acids. It could be observed that the nature of substituents (electron-releasing or electron-withdrawing) on the benzylic alcohols had an explicit impact on the oxidation rate. Benzylic alcohols bearing electron-releasing groups were found to be more active and were oxidized to the respective aldehydes in shorter reaction periods. The rate of the oxidation process was slower when the benzyl alcohol contained an electron-withdrawing group. That might be ascribed to the decrease of electronic cloud density on the aromatic ring caused by -ve induction effect [52]. Additionally, it was observed that the *para*-substituted benzyl alcohols were easily oxidized by comparing with the *ortho*- and *meta*-substituted alcohols, presumably because the *para*-derivative has lower steric hindrance by comparing with other derivatives [53]. In this regard, *p*-methylbenzyl alcohol was wholly converted to *p*-methylbenzaldehyde within only 35 min (Table S1, entry 3), whereas *o*- and *m*-methylbenzyl alcohol were fully oxidized within longer times of 45 and 50 min, correspondingly (Table S1, entries 7 and 10). It was also found that the steric hindrance had a significant effect on the oxidation rate; the bulk group (e.g., trifluoromethyl, trimethoxy, dichloro, and pentafluoro) connected to benzyl alcohol reduced the efficiency of the oxidation process, might be owing to the steric hindrance that prohibited oxidation of the alcohols possessing bulk groups (Table S1, entries 17–20) [54]. It is noteworthy to mention that cinnamyl alcohol, as an example of allylic alcohol, achieved 100% conversion and <99% selectivity of cinnamaldehyde within 50 min (Table S1, entry 21). The furfuryl alcohol, as an example of hetero-aromatic alcohol, was also wholly transformed to furfural after 110 min (Table S1, entry 22). Moreover, the current catalytic methodology was also applicable to the oxidation of secondary benzylic alcohols, and complete convertibility and selectivity to the respective ketone derivatives was achieved at the same circumstances (Table S1, entries 23–28).

Indeed, the oxygenation of aliphatic alcohols is significantly more complicated with respect to the aromatic counterparts [55], and excellent results are obtained by oxidation of primary aliphatic alcohols using the present catalytic strategy. In this regard, the oxidation of cyclohexyl methanol, 5-hexenol,

1-octanol, and citronellol into their corresponding aliphatic aldehydes took place in relatively longer reaction times (Table S1, entries 29–32). Compared to secondary benzylic alcohols, the oxidation of secondary aliphatic alcohols showed a lower reactivity towards this oxidation transformation (Table S1, entries 33–35). Obviously, it was indispensable to elongate the time because the oxidation of benzylic secondary alcohols was easier than that of aliphatic ones. As estimated, full oxidation of  $\alpha$ -phenyl-ethanol occurred within only 25 min, while the entire oxidation of 2-octanol occurred after a long time of 240 min (Table S1, entries 25 and 35). Accordingly, the present catalytic methodology was impacted by dual factors—electronic and steric impacts. As a conclusion, in general, the current catalytic oxidation protocol was found to be efficacious for oxygenation of various kinds of alcohols, including benzylic, aliphatic, allylic, heterocyclic, primary, and secondary alcohols, indicating the versatility of  $\text{Ag}_2\text{O}-\text{MnO}_2/(5 \text{ wt.}\%)\text{GRO}$  catalyst for aerial selective alcohol oxidation.

### 3. Experimental

#### 3.1. Synthesis of GRO

Initially, GRO was fabricated from pristine graphite through Hummer's method [56].

#### 3.2. Synthesis of $\text{Ag}_2\text{O}-\text{MnO}_2$ Nanoparticles

The  $\text{Ag}_2\text{O}-\text{MnO}_2$  was prepared separately through a co-precipitation procedure. In brief, stoichiometric amounts of  $\text{AgNO}_3$  and  $\text{Mn}(\text{NO}_3)_2$  were dissolved in distilled water (100 mL), followed by the dropwise addition of 0.5 M  $\text{NaHCO}_3$  solution at 100 °C for 3 h (till the pH of the resultant solution reached to 9). The vigorous stirring of the resultant mixture was continued overnight at RT. The reaction mixture was filtered via centrifugation and dried at 70 °C for 12 h. The as-obtained nanomaterial was annealed at 300 °C for 24 h and further used for the preparation of nanocomposite. Subsequently, the previously prepared GRO, dried at 70 °C, was introduced in the  $\text{Ag}_2\text{O}-\text{MnO}_2$  by milling to synthesize the desired (1%)  $\text{Ag}_2\text{O}-\text{MnO}_2/\text{GRO}$  catalyst. It is important to note that if GRO was incorporated before the calcination process, there was a significant decrease in weight and catalytic activity.

#### 3.3. Synthesis of $\text{Ag}_2\text{O}-\text{MnO}_2/\text{GRO}$ Nanocomposite

For this purpose, the GRO was prepared using a previously reported modified Hummer's method using natural graphite and dried overnight at 40 °C. Approximately, 1.90 g of  $\text{Ag}_2\text{O}-\text{MnO}_2$  nanoparticles and 0.1 g of GRO powder were milled using Fritsch Pulverisette P7 (Idar-Oberstein, Germany) planetary ball mill. The graphite oxide powder and stainless steel balls (5 mm diameter) with the ball to powder weight ratio of 11:1 were introduced into the stainless steel container. The milling of the powder was performed for 16 h. In order to maintain the temperature inside the container, the milling process was paused at regular intervals.

#### 3.4. Catalyst Characterization

The prepared materials were characterized using several instruments, and all experimental details are described in the supplementary file.

#### 3.5. Catalytic Assessment

Oxidation of benzyl alcohol was performed in a glass flask equipped with a magnetic stirrer, reflux condenser, and thermometer. A mixture of benzyl alcohol (2 mmol), toluene (10 mL), and the catalyst (0.3 g) was transferred in a glass three-necked round-bottomed flask; the resulting mixture was then heated to the desired temperature with vigorous stirring. The oxidation experiment was started by bubbling  $\text{O}_2$  gas at a flow rate of  $20 \text{ mL}\cdot\text{min}^{-1}$  into the reaction mixture. After the reaction, the solid catalyst was filtered off by centrifugation, and the liquid products were analyzed by gas chromatography to determine the conversion of the alcohol and product selectivity by (GC, 7890A)



Agilent Technologies Inc (Santa Clara, CA, United States), equipped with a flame ionization detector (FID) and a 19019S-001 HP-PONA column.

### 3.6. Reusability Tests

After the completion of the first oxidation process, the used catalyst was separated by centrifugation (HERMLE Labortechnik GmbH, · Wehingen, Germany ), then washed many times with toluene and dried at 95 °C for 5 h for the next run. The dried catalyst was used for the next run under similar aforementioned conditions.

## 4. Conclusions

Herein, we reported a cost-effective and eco-friendly mechanochemical approach for the preparation of GRO-based  $\text{Ag}_2\text{O-MnO}_2$  nanocatalyst for the aerial oxidation of a variety of alcohols. The nanocatalyst demonstrated a high conversion ability ( $\sim 100\%$ ) and excellent selectivity in the presence of  $\text{O}_2$  as a clean oxidant without utilizing any hazardous surfactants or bases. Under the optimum conditions,  $(1\%)\text{Ag}_2\text{O-MnO}_2/(5 \text{ wt.}\%)\text{GRO}$  catalyst exhibited better catalytic performance ( $100\%$  conversion) in comparison with  $\text{Ag}_2\text{O-MnO}_2$  catalyst. The higher catalytic properties of the nanocomposite were attributed to the presence of GRO, which exhibited extraordinary catalytic properties like high surface area, excellent chemical compatibility and stability, superior mechanical and thermal stability, as well as the presence of several defects. The eco-friendly, physical blending of the components, including GRO and  $\text{Ag}_2\text{O-MnO}_2$  NPs, at RT avoided the pyrolysis of oxygen-containing functional groups, which allowed to preserve the defects and active sites of the resulting composite. Therefore,  $(1\%)\text{Ag}_2\text{O-MnO}_2/(5 \text{ wt.}\%)\text{GRO}$  showed a  $100\%$  conversion of  $\text{BnOH}$  with  $\sim 99\%$  selectivity towards the formation of  $\text{BnH}$  within a relatively short time. The obtained specific performance ( $13.3 \text{ mmol}\cdot\text{g}^{-1}\cdot\text{h}^{-1}$ ) was much better than that presented in previous literature. Our catalytic strategy was highly selective, producing only desired products with no over-oxygenation to carboxylic acids. The merits of our catalytic methodology were: (a) facile process, (b) inexpensive and clean oxidant, (c) no surfactants or nitrogenous bases were required, (d) mild catalytic conditions, (e) cost-effective recoverable catalyst, (f) complete convertibility, (g) full selectivity, (h) rapid process, and (i) applicable to virtually all types of alcohols. So, these highlights made this catalytic strategy to be highly applicable in the industrial applications for manufacturing of carbonyls.

**Supplementary Materials:** The following are available online at <http://www.mdpi.com/2073-4344/10/3/281/s1>, Figure S1: FTIR spectrum of GRO and  $(1\%)\text{Ag}_2\text{O-MnO}_2/(5 \text{ wt.}\%)\text{GRO}$  nanocomposite. Table S1: Aerial oxidation of several kinds of alcohols using  $\text{Ag}_2\text{O-MnO}_2/(5 \text{ wt.}\%)\text{GRO}$  with  $\text{O}_2$  under alkali free conditions.

**Author Contributions:** S.F.A. designed the project; M.E.A., M.K. (Mujeeb Khan), and M.R.S. helped to write the manuscript; M.E.A. and M.K. (Mufsir Kuniyil) performed the experimental section and some part of characterization; D.S. and A.Z.D. performed some part of characterization; A.A.-W. and M.R.H.S. provided scientific guidance for the successful completion of the project and helped to draft the manuscript. All authors have read and agreed to the published version of the manuscript.

**Funding:** This research and APC was funded by Deanship of Scientific Research, King Saud University, Research group project No. RG-1436-032.

**Acknowledgments:** The authors extend their appreciation to the Deanship of Scientific Research at King Saud University for funding this work through the research group project No. RG-1436-032.

**Conflicts of Interest:** The authors declare no conflict of interest.

## References

1. Kolobova, E.; Kotolevich, Y.; Pakrieva, E.; Mamontov, G.; Farias, M.; Corberán, V.C.; Bogdanchikova, N.; Hemming, J.; Smeds, A.; Mäki-Arvela, P. Modified  $\text{Ag/TiO}_2$  systems: Promising catalysts for liquid-phase oxidation of alcohols. *Fuel* **2018**, *234*, 110–119. [CrossRef]
2. Faqeeh, A.J.; Ali, T.T.; Basahel, S.N.; Narasimharao, K. Nanosized samarium modified  $\text{Au-Ce}_{0.5}\text{Zr}_{0.5}\text{O}_2$  catalysts for oxidation of benzyl alcohol. *Mol. Catal.* **2018**, *456*, 10–21. [CrossRef]

3. Liu, K.; Qin, T.; Sun, Y.; Hou, C.; Cao, X.; Jiang, S. Synergistic effect between Ag and Mn<sub>3</sub>O<sub>4</sub> in the gas phase oxidation of alcohols. *Catal. Commun.* **2018**, *113*, 15–18. [[CrossRef](#)]
4. Dai, X.; Rasamani, K.D.; Wu, S.; Sun, Y. Enabling selective aerobic oxidation of alcohols to aldehydes by hot electrons in quantum-sized Rh nanocubes. *Mater. Today Energy* **2018**, *10*, 15–22. [[CrossRef](#)]
5. Biella, S.; Rossi, M. Gas phase oxidation of alcohols to aldehydes or ketones catalysed by supported gold. *Chem. Commun.* **2003**, 378–379. [[CrossRef](#)]
6. Khan, M.; Tahir, M.N.; Adil, S.F.; Khan, H.U.; Siddiqui, M.R.H.; Al-warthan, A.A.; Tremel, W. Graphene based metal and metal oxide nanocomposites: Synthesis, properties and their applications. *J. Mater. Chem. A* **2015**, *3*, 18753–18808. [[CrossRef](#)]
7. Loh, K.P.; Bao, Q.; Ang, P.K.; Yang, J. The chemistry of graphene. *J. Mater. Chem.* **2010**, *20*, 2277–2289. [[CrossRef](#)]
8. Fan, X.; Zhang, G.; Zhang, F. Multiple roles of graphene in heterogeneous catalysis. *Chem. Soc. Rev.* **2015**, *44*, 3023–3035. [[CrossRef](#)]
9. Su, C.; Loh, K.P. Carbocatalysts: Graphene oxide and its derivatives. *Acc. Chem. Res.* **2013**, *46*, 2275–2285. [[CrossRef](#)]
10. Su, C.; Acik, M.; Takai, K.; Lu, J.; Hao, S.-j.; Zheng, Y.; Wu, P.; Bao, Q.; Enoki, T.; Chabal, Y.J. Probing the catalytic activity of porous graphene oxide and the origin of this behaviour. *Nat. Commun.* **2012**, *3*, 1298. [[CrossRef](#)]
11. Ali, A.A.; Madkour, M.; Sagheer, F.A.; Zaki, M.I.; Abdel Nazeer, A. Low-Temperature Catalytic CO Oxidation Over Non-Noble, Efficient Chromia in Reduced Graphene Oxide and Graphene Oxide Nanocomposites. *Catalysts* **2020**, *10*, 105. [[CrossRef](#)]
12. Gopiraman, M.; Saravanamoorthy, S.; Deng, D.; Ilangoan, A.; Kim, I.S.; Chung, I.M. Facile mechanochemical synthesis of nickel/graphene oxide nanocomposites with unique and tunable morphology: Applications in heterogeneous catalysis and supercapacitors. *Catalysts* **2019**, *9*, 486. [[CrossRef](#)]
13. Sun, W.; Lu, X.; Tong, Y.; Zhang, Z.; Lei, J.; Nie, G.; Wang, C. Fabrication of highly dispersed palladium/graphene oxide nanocomposites and their catalytic properties for efficient hydrogenation of p-nitrophenol and hydrogen generation. *Int. J. Hydrogen Energy* **2014**, *39*, 9080–9086. [[CrossRef](#)]
14. Shao, L.; Huang, X.; Teschner, D.; Zhang, W. Gold supported on graphene oxide: An active and selective catalyst for phenylacetylene hydrogenations at low temperatures. *ACS Catal.* **2014**, *4*, 2369–2373. [[CrossRef](#)]
15. Xu, C.; Wang, X.; Zhu, J.; Yang, X.; Lu, L. Deposition of Co<sub>3</sub>O<sub>4</sub> nanoparticles onto exfoliated graphite oxide sheets. *J. Mater. Chem.* **2008**, *18*, 5625–5629. [[CrossRef](#)]
16. Adil, S.F.; Assal, M.E.; Shaik, M.R.; Kuniyil, M.; AlOtaibi, N.M.; Khan, M.; Sharif, M.; Alam, M.M.; Al-Warthan, A.; Mohammed, J.A. A Facile Synthesis of ZrO<sub>x</sub>-MnCO<sub>3</sub>/Graphene Oxide (GRO) Nanocomposites for the Oxidation of Alcohols using Molecular Oxygen under Base Free Conditions. *Catalysts* **2019**, *9*, 759. [[CrossRef](#)]
17. Liu, Y.; Jin, W.; Zhao, Y.; Zhang, G.; Zhang, W. Enhanced catalytic degradation of methylene blue by  $\alpha$ -Fe<sub>2</sub>O<sub>3</sub>/graphene oxide via heterogeneous photo-Fenton reactions. *Appl. Catal. B Environ.* **2017**, *206*, 642–652. [[CrossRef](#)]
18. Assal, M.E.; Shaik, M.R.; Kuniyil, M.; Khan, M.; Al-Warthan, A.; Siddiqui, M.R.H.; Khan, S.M.; Tremel, W.; Tahir, M.N.; Adil, S.F. A highly reduced graphene oxide/ZrO<sub>x</sub>-MnCO<sub>3</sub> or-Mn<sub>2</sub>O<sub>3</sub> nanocomposite as an efficient catalyst for selective aerial oxidation of benzylic alcohols. *RSC Adv.* **2017**, *7*, 55336–55349. [[CrossRef](#)]
19. Arumugam, S.; Mohan, B.C.; Vasudevan, S.V.; Vanaraj, R.; Rukmanikrishnan, B.; Periyasamy, T.; Asrafali, S.P. Selective Oxidation of Cyclohexane Using Graphene Oxide-Supported Ceria Nanocomposites with Exposed Active {1 0 0} Facets. *ChemistrySelect* **2017**, *2*, 6223–6230. [[CrossRef](#)]
20. Zhao, B.; Liu, J.; Zhou, L.; Long, D.; Feng, K.; Sun, X.; Zhong, J. Probing the electronic structure of M-graphene oxide (M= Ni, Co, NiCo) catalysts for hydrolytic dehydrogenation of ammonia borane. *Appl. Surf. Sci.* **2016**, *362*, 79–85. [[CrossRef](#)]
21. Wang, C.; Hu, L.; Hu, Y.; Ren, Y.; Chen, X.; Yue, B.; He, H. Direct hydroxylation of benzene to phenol over metal oxide supported graphene oxide catalysts. *Catal. Commun.* **2015**, *68*, 1–5. [[CrossRef](#)]
22. Diao, J.; Liu, H.; Wang, J.; Feng, Z.; Chen, T.; Miao, C.; Yang, W.; Su, D.S. Porous graphene-based material as an efficient metal free catalyst for the oxidative dehydrogenation of ethylbenzene to styrene. *Chem. Commun.* **2015**, *51*, 3423–3425. [[CrossRef](#)] [[PubMed](#)]
23. Zhao, Q.; Bai, C.; Zhang, W.; Li, Y.; Zhang, G.; Zhang, F.; Fan, X. Catalytic epoxidation of olefins with graphene oxide supported copper (Salen) complex. *Ind. Eng. Chem. Res.* **2014**, *53*, 4232–4238. [[CrossRef](#)]

24. Al-Marri, A.H.; Khan, M.; Shaik, M.R.; Mohri, N.; Adil, S.F.; Kuniyil, M.; Alkhathlan, H.Z.; Al-Warthan, A.; Tremel, W.; Tahir, M.N. Green Synthesis of Pd@ Graphene Nanocomposite: Catalyst for the Selective Oxidation of Alcohols. *Arab. J. Chem.* **2016**, *9*, 835–845. [\[CrossRef\]](#)
25. Al-Marri, A.H.; Khan, M.; Khan, M.; Adil, S.F.; Al-Warthan, A.; Alkhathlan, H.Z.; Tremel, W.; Labis, J.P.; Siddiqui, M.R.H.; Tahir, M.N. Pulicaria glutinosa extract: A toolbox to synthesize highly reduced graphene oxide-silver nanocomposites. *Int. J. Mol. Sci.* **2015**, *16*, 1131–1142. [\[CrossRef\]](#)
26. Rincon, E.; Garcia, A.; Romero, A.A.; Serrano, L.; Luque, R.; Balu, A.M. Mechanochemical preparation of novel polysaccharide-supported Nb<sub>2</sub>O<sub>5</sub> catalysts. *Catalysts* **2019**, *9*, 38. [\[CrossRef\]](#)
27. Zhao, B.; Zheng, Y.; Ye, F.; Deng, X.; Xu, X.; Liu, M.; Shao, Z. Multifunctional iron oxide nanoflake/graphene composites derived from mechanochemical synthesis for enhanced lithium storage and electrocatalysis. *ACS Appl. Mater. Interfaces* **2015**, *7*, 14446–14455. [\[CrossRef\]](#)
28. Assal, M.E.; Shaik, M.R.; Kuniyil, M.; Khan, M.; Al-Warthan, A.; Alharthi, A.I.; Varala, R.; Siddiqui, M.R.H.; Adil, S.F. Ag<sub>2</sub>O nanoparticles/MnCO<sub>3</sub>–MnO<sub>2</sub> or–Mn<sub>2</sub>O<sub>3</sub>/highly reduced graphene oxide composites as an efficient and recyclable oxidation catalyst. *Arab. J. Chem.* **2019**, *12*, 54–68. [\[CrossRef\]](#)
29. Sandhya, P.K.; Jose, J.; Sreekala, M.S.; Padmanabhan, M.; Kalarikkal, N.; Thomas, S. Reduced graphene oxide and ZnO decorated graphene for biomedical applications. *Ceram. Int.* **2018**, *44*, 15092–15098. [\[CrossRef\]](#)
30. Ma, Z.; Yu, T.; Bi, L. Ru-containing polyoxometalate fabricated on graphene oxide: Preparation, characterization and catalytic activity. *J. Solid State Chem.* **2019**, *275*, 16–22. [\[CrossRef\]](#)
31. Vithalani, R.; Patel, D.; Modi, C.K.; Som, N.N.; Jha, P.K.; Kane, S. Enhancing the potency of surface hydroxyl groups of graphene oxide for selective oxidation of benzyl alcohol. *Diam. Relat. Mater.* **2018**, *90*, 154–165. [\[CrossRef\]](#)
32. Assal, M.E.; Shaik, M.R.; Kuniyil, M.; Khan, M.; Kumar, J.; Alzahrani, A.Y.; Al-Warthan, A.; Al-Tamrah, S.A.; Siddiqui, M.R.H.; Hashmi, S.A. Silver-doped manganese based nanocomposites for aerial oxidation of alcohols. *Mater. Express* **2018**, *8*, 35–54. [\[CrossRef\]](#)
33. Santra, S.; Hota, P.K.; Bhattacharyya, R.; Bera, P.; Ghosh, P.; Mandal, S.K. Palladium nanoparticles on graphite oxide: A recyclable catalyst for the synthesis of biaryl cores. *ACS Catal.* **2013**, *3*, 2776–2789. [\[CrossRef\]](#)
34. Wang, Z.-l.; Xu, D.; Huang, Y.; Wu, Z.; Wang, L.-m.; Zhang, X.-b. Facile, mild and fast thermal-decomposition reduction of graphene oxide in air and its application in high-performance lithium batteries. *Chem. Commun.* **2012**, *48*, 976–978. [\[CrossRef\]](#) [\[PubMed\]](#)
35. Geng, L.; Wu, S.; Zou, Y.; Jia, M.; Zhang, W.; Yan, W.; Liu, G. Correlation between the microstructures of graphite oxides and their catalytic behaviors in air oxidation of benzyl alcohol. *J. Colloid Interface Sci.* **2014**, *421*, 71–77. [\[CrossRef\]](#) [\[PubMed\]](#)
36. Metin, Ö.; Kayhan, E.; Özkaz, S.; Schneider, J.J. Palladium nanoparticles supported on chemically derived graphene: An efficient and reusable catalyst for the dehydrogenation of ammonia borane. *Int. J. Hydrogen Energy* **2012**, *37*, 8161–8169. [\[CrossRef\]](#)
37. Han, G.; Liu, Y.; Kan, E.; Tang, J.; Zhang, L.; Wang, H.; Tang, W. Sandwich-structured MnO<sub>2</sub>/polypyrrole/reduced graphene oxide hybrid composites for high-performance supercapacitors. *Rsc Adv.* **2014**, *4*, 9898–9904. [\[CrossRef\]](#)
38. Gil, S.; Muñoz, L.; Sánchez-Silva, L.; Romero, A.; Valverde, J.L. Synthesis and characterization of Au supported on carbonaceous material-based catalysts for the selective oxidation of glycerol. *Chem. Eng. J.* **2011**, *172*, 418–429. [\[CrossRef\]](#)
39. Liu, S.; Yan, J.; He, G.; Zhong, D.; Chen, J.; Shi, L.; Zhou, X.; Jiang, H. Layer-by-layer assembled multilayer films of reduced graphene oxide/gold nanoparticles for the electrochemical detection of dopamine. *J. Electroanal. Chem.* **2012**, *672*, 40–44. [\[CrossRef\]](#)
40. Rajesh, D.; Mahendiran, C.; Suresh, C.; Pandurangan, A.; Maiyalagan, T. Hydrothermal synthesis of three dimensional reduced graphene oxide-multiwalled carbon nanotube hybrids anchored with palladium-cerium oxide nanoparticles for alcohol oxidation reaction. *Int. J. Hydrogen Energy* **2019**, *44*, 4962–4973. [\[CrossRef\]](#)
41. Hu, Z.; Zhao, Y.; Liu, J.; Wang, J.; Zhang, B.; Xiang, X. Ultrafine MnO<sub>2</sub> nanoparticles decorated on graphene oxide as a highly efficient and recyclable catalyst for aerobic oxidation of benzyl alcohol. *J. Colloid Interface Sci.* **2016**, *483*, 26–33. [\[CrossRef\]](#) [\[PubMed\]](#)
42. Wu, G.; Wang, X.; Guan, N.; Li, L. Palladium on graphene as efficient catalyst for solvent-free aerobic oxidation of aromatic alcohols: Role of graphene support. *Appl. Catal. B Environ.* **2013**, *136*, 177–185. [\[CrossRef\]](#)

43. Yu, X.; Huo, Y.; Yang, J.; Chang, S.; Ma, Y.; Huang, W. Reduced Graphene Oxide Supported Au Nanoparticles as an Efficient Catalyst for Aerobic Oxidation of Benzyl Alcohol. *Appl. Surf. Sci.* **2013**, *280*, 450–455. [CrossRef]
44. Rana, S.; Jonnalagadda, S.B. Cu doped amine functionalized graphene oxide and its scope as catalyst for selective oxidation. *Catal. Commun.* **2017**, *100*, 183–186. [CrossRef]
45. Feng, X.; Lv, P.; Sun, W.; Han, X.; Gao, L.; Zheng, G. Reduced graphene oxide-supported Cu nanoparticles for the selective oxidation of benzyl alcohol to aldehyde with molecular oxygen. *Catal. Commun.* **2017**, *99*, 105–109. [CrossRef]
46. Ramirez-Barria, C.S.; Isaacs, M.; Parlett, C.; Wilson, K.; Guerrero-Ruiz, A.; Rodríguez-Ramos, I. Ru nanoparticles supported on N-doped reduced graphene oxide as valuable catalyst for the selective aerobic oxidation of benzyl alcohol. *Catal. Today* **2019**. [CrossRef]
47. Zahed, B.; Hosseini-Monfared, H. A comparative study of silver-graphene oxide nanocomposites as a recyclable catalyst for the aerobic oxidation of benzyl alcohol: Support effect. *Appl. Surf. Sci.* **2015**, *328*, 536–547. [CrossRef]
48. Zhang, W.-H.; Shen, J.-J.; Wu, J.; Liang, X.-Y.; Xu, J.; Liu, P.; Xue, B.; Li, Y.-X. An amphiphilic graphene oxide-immobilized polyoxometalate-based ionic liquid: A highly efficient triphase transfer catalyst for the selective oxidation of alcohols with aqueous H<sub>2</sub>O<sub>2</sub>. *Mol. Catal.* **2017**, *443*, 262–269. [CrossRef]
49. Jha, A.; Mhamane, D.; Suryawanshi, A.; Joshi, S.M.; Shaikh, P.; Biradar, N.; Ogale, S.; Rode, C.V. Triple nanocomposites of CoMn<sub>2</sub>O<sub>4</sub>, Co<sub>3</sub>O<sub>4</sub> and reduced graphene oxide for oxidation of aromatic alcohols. *Catal. Sci. Technol.* **2014**, *4*, 1771–1778. [CrossRef]
50. Liu, K.; Chen, T.; Hou, Z.; Wang, Y.; Dai, L. Graphene Oxide as Support for the Immobilization of Phosphotungstic Acid: Application in the Selective Oxidation of Benzyl Alcohol. *Catal. Lett.* **2014**, *144*, 314–319. [CrossRef]
51. Rana, S.; Maddila, S.; Jonnalagadda, S.B. Synthesis and characterization of Pd (II) dispersed over diamine functionalized graphene oxide and its scope as a catalyst for selective oxidation. *Catal. Sci. Technol.* **2015**, *5*, 3235–3241. [CrossRef]
52. Xu, C.; Zhang, L.; An, Y.; Wang, X.; Xu, G.; Chen, Y.; Dai, L. Promotional synergistic effect of Sn doping into a novel bimetallic Sn-W oxides/graphene catalyst for selective oxidation of alcohols using aqueous H<sub>2</sub>O<sub>2</sub> without additives. *Appl. Catal. A Gen.* **2018**, *558*, 26–33. [CrossRef]
53. Hosseini-Sarvari, M.; Ataee-Kachouei, T.; Moeini, F. A novel and active catalyst Ag/ZnO for oxidant-free dehydrogenation of alcohols. *Mater. Res. Bull.* **2015**, *72*, 98–105. [CrossRef]
54. Borthakur, R.; Asthana, M.; Kumar, A.; Lal, R.A. Cooperative Catalysis by Polymetallic Copper–Zinc Complexes in the Efficient Oxidation of Alcohols under Solvent Free Condition. *Inorg. Chem. Commun.* **2014**, *46*, 198–201. [CrossRef]
55. Assady, E.; Yadollahi, B.; Riahi Farsani, M.; Moghadam, M. Zinc polyoxometalate on activated carbon: An efficient catalyst for selective oxidation of alcohols with hydrogen peroxide. *Appl. Organomet. Chem.* **2015**, *29*, 561–565. [CrossRef]
56. Hummers, W.S., Jr.; Offeman, R.E. Preparation of graphitic oxide. *J. Am. Chem. Soc.* **1958**, *80*, 1339. [CrossRef]

